Comparative analysis of spectral coherence in microresonator frequency combs

Comparative analysis of spectral coherence in microresonator frequency combs

Victor Torres-Company,[1] **David Castelló-Lurbe,**[2] **and Enrique Silvestre**[2,*]

[1]*Department of Microtechnology and Nanoscience, Chalmers University of Technology, SE-41296 Gothenburg, Sweden*
[2]*Departament d'Òptica, Universitat de València, 46100 Burjassot, Spain*
[*]*enrique.silvestre@uv.es*

Abstract: Microresonator combs exploit parametric oscillation and nonlinear mixing in an ultrahigh-Q cavity. This new comb generator offers unique potential for chip integration and access to high repetition rates. However, time-domain studies reveal an intricate spectral coherence behavior in this type of platform. In particular, coherent, partially coherent or incoherent combs have been observed using the same microresonator under different pumping conditions. In this work, we provide a numerical analysis of the coherence dynamics that supports the above experimental findings and verify particular design rules to achieve spectrally coherent microresonator combs. A particular emphasis is placed in understanding the differences between so-called Type I and Type II combs.

OCIS codes: (320.7110) Ultrafast nonlinear optics; (030.1640) Coherence; (130.3990) Micro-optical devices.

References and links

1. D. J. Jones, S. A. Diddams, J. K. Ranka, A. Stentz, R. S. Windeler, J. L. Hall, and S. T. Cundiff, "Carrier-envelope phase control of femtosecond mode-locked lasers and direct optical frequency synthesis," Science **288**, 635–639 (2000).
2. S. A. Diddams, D. J. Jones, J. Ye, S. T. Cundiff, J. L. Hall, J. K. Ranka, R. S. Windeler, R. Holzwarth, T. Udem, and T. W. Hänsch, "Direct link between microwave and optical frequencies with a 300 THz femtosecond laser comb," Phys. Rev. Lett. **84**, 5102–5105 (2000).
3. T. W. Hänsch, "Nobel Lecture: Passion for precision," Rev. Mod. Phys. **78**, 1297–1309 (2006).
4. N. R. Newbury, "Searching for applications with a fine-tooth comb," Nature Photon. **5**, 186–188 (2011).
5. V. Torres-Company and A. M. Weiner, "Optical frequency comb technology for ultra-broadband radio-frequency photonics," Laser and Photon. Rev. (in press, 2013). DOI 10.1002/lpor201300126.
6. T. J. Kippenberg, R. Holzwarth, and S. A. Diddams, "Microresonator-based optical frequency combs," Science **332**, 555–559 (2011).
7. P. Del'Haye, A. Schliesser, O. Arcizet, T. Wilken, R. Holzwarth, and T. J. Kippenberg, "Optical frequency comb generation from a monolithic microresonator," Nature **450**, 1214–1217 (2007).
8. A. A. Savchenkov, A. B. Matsko, V. S. Ilchenko, I. Solomatine, D. Seidel, and L. Maleki, "Tunable optical frequency comb with a crystalline whispering gallery mode resonator," Phys. Rev. Lett. **101**, 093902 (2008).
9. W. Liang, A. A. Savchenkov, A. B. Matsko, V. S. Ilchenko, D. Seidel, and L. Maleki, "Generation of near-infrared frequency combs from a MgF2 whispering gallery mode resonator," Opt. Lett. **36**, 2290–2292 (2011).
10. L. Razzari, D. Duchesne, M. Ferrera, R. Morandotti, S. Chu, B. E. Little, and D. J. Moss, "CMOS-compatible integrated optical hyper-parametric oscillator," Nat. Photonics **4**, 41–45 (2010).
11. J. S. Levy, A. Gondarenko, M. A. Foster, A. C. Turner-Foster, A. L. Gaeta, and M. Lipson, "CMOS-compatible multiple-wavelength oscillator for on-chip optical interconnects," Nat. Photonics **4**, 37–40 (2010).

#203476 - $15.00 USD Received 26 Dec 2013; revised 8 Feb 2014; accepted 13 Feb 2014; published 20 Feb 2014

12. H. Jung, C. Xiong, K. Y. Fong, X. F. Zhang, and H. X. Tang, "Optical frequency comb generation from aluminum nitride microring resonator," Opt. Lett. **38**, 2810–2813 (2013).
13. Y. Okawachi, K. Saha, J. S. Levy, Y. H. Wen, M. Lipson, and A. L. Gaeta, "Octave-spanning frequency comb generation in a silicon nitride chip," Opt. Lett. **36**, 3398–3400 (2011).
14. P. Del'Haye, T. Herr, E. Garvatin, M. L. Gorodetsky, R. Holzwarth, and T. J. Kippenberg, "Octave spanning tunable frequency comb from a microresonator," Phys. Rev. Lett. **107**, 063901 (2011).
15. M. A. Foster, A. C. Turner, R. Salem, M. Lipson, and A. L. Gaeta, "Broad-band continuous-wave parametric wavelength conversion in silicon nanowaveguides," Opt. Express **15**, 12949–12958 (2007).
16. L. Zhang, Y. Yue, R. G. Beausoleil, and A. E. Willner, "Analysis and engineering of chromatic dispersion in silicon waveguide bends and ring resonators," Opt. Express **19**, 8102–8107 (2011).
17. J. Riemensberger, K. Hartinger, T. Herr, V. Brasch, R. Holzwarth, and T. J. Kippenberg, "Dispersion engineering of thick high-Q silicon nitride ring-resonators via atomic layer deposition," Opt. Express **20**, 27661–27669 (2012).
18. I. S. Grudinin, L. Baumgartel, and N. Yu, "Frequency comb from a microresonator with engineered spectrum," Opt. Express **20**, 6604–6609 (2012).
19. J. Li, H. Lee, T. Chen, and K. J. Vahala, "Low-pump-power, low-phase-noise, and microwave to millimeter-wave repetition rate operation in microcombs," Phys. Rev. Lett. **109**, 233901 (2012).
20. A. A. Savchenko, A. B. Matsko, W. Liang, V. S. Ilchenko, D. Seidel, L. Maleki, "Kerr combs with selectable central frequency," Nature Photon. **5**, 293–296 (2011).
21. K. Saha, Y. Okawachi, J. S. Levy, R. K. W. Lau, K. Luke, M. A. Foster, M. Lipson, and A. L. Gaeta, "Broadband parametric frequency comb generation with a 1 μm pump source," Opt. Express **20**, 26935–26941 (2012).
22. C. Y. Wang, T. Herr, P. Del'Haye, A. Schliesser, J. Hofer, R. Holzwarth, T. W. Hänsch, N. Picque, and T. J. Kippenberg, "Mid-infrared optical frequency combs at 2.5 μm based on crystalline microresonators," Nature Commun. **4**, 1345 (2013).
23. D. J. Moss, R. Morandotti, A. L. Gaeta, and M. Lipson, "New CMOS-compatible platforms based on silicon nitride and Hydex for nonlinear optics," Nat. Photonics **7**, 597–607 (2013).
24. F. Ferdous, H. X Miao, D. E. Leaird, K. Srinivasan, J. Wang, L. Chen, L. T. Varghese, and A. M. Weiner, "Spectral line-by-line pulse shaping of on-chip microresonator frequency combs," Nat. Photonics **5**, 770–776 (2011).
25. S. B. Papp and S. A. Diddams, "Spectral and temporal characterization of a fused-quartz-microresonator optical frequency comb," Phys. Rev. A **84**, 053833 (2011).
26. S. T. Cundiff and A. M. Weiner, "Optical arbitrary waveform generation," Nat. Photonics **4**, 760–766 (2010).
27. F. Ferdous, H. X. Miao, P. H. Wang, D. E. Leaird, K. Srinivasan, L. Chen, V. Aksyuk, and A. M. Weiner, "Probing coherence in microcavity frequency combs via optical pulse shaping," Opt. Express **20**, 21033–21043 (2012).
28. P. H. Wang, F. Ferdous, H. X Miao, J. Wang, D. E. Leaird, K. Srinivasan, L. Chen, V. Aksyuk, and A. M. Weiner, "Observation of correlation between route to formation, coherence, noise, and communication performance of Kerr combs," Opt. Express **20**, 29284–29295 (2012).
29. T. Herr, K. Hartinger, J. Riemesberger, C. Y. Wang, E. Gavartin, R. Holzwarth, M. L. Gorodetsky, and T. J. Kippenberg, "Universal formation dynamics and noise of Kerr-frequency combs in microresonators," Nat. Photonics **6**, 480–487 (2012).
30. A. B. Matsko, A. A. Savchenko, D. Strekalov, V. S. Ilchenko, and L. Maleki, "Optical hyperparametric oscillations in a whispering-gallery-mode resonator: Threshold and phase diffusion," Phys. Rev. A **71**, 033804 (2005).
31. Y. K. Chembo and N. Yu, "Modal expansion approach to optical-frequency-comb generation with monolithic whispering-gallery-mode resonators," Phys. Rev. A **82**, 033801 (2010).
32. A. B. Matsko, A. A. Savchenko, W. Liang, V. S. Ilchenko, D. Seidel, and L. Maleki, "Mode-locked Kerr frequency combs," Opt. Lett. **36**, 2845–2847 (2011).
33. A. B. Matsko, A. A. Savchenko, V. S. Ilchenko, D. Seidel, and L. Maleki, "Hard and soft excitation regimes of Kerr frequency combs," Phys. Rev. A **85**, 023830 (2012).
34. Y. K. Chembo and C. R. Menyuk, "Spatiotemporal Lugiato-Lefever formalism for Kerr-comb generation in whispering gallery-mode resonators," Phys. Rev. A **87**, 053852 (2013).
35. S. Coen, H. G. Randle, T. Sylvestre, and M. Erkintalo "Modeling of octave-spanning Kerr frequency combs using a generalized mean-field Lugiato-Lefever model," Opt. Lett. **38**, 37–39 (2013).
36. T. Hansson, D. Modotto, and S. Wabnitz, "Dynamics of the modulation instability in microresonator frequency combs," Phys. Rev. A **88**, 023819 (2013).
37. C. Godey, I. Balakireva, A. Colleit, and Y. K Chembo, "Stability analysis of the Lugiato-Lefever model for Kerr optical frequency combs. Part I: case of normal dispersion," arXiv: 1308.2539.
38. S. Coen and M. Erkintalo, "Universal scaling laws of Kerr frequency combs," Opt. Lett. **38**, 1790–1792 (2013).
39. A. B. Matsko, W. Liang, A. A. Savchenko, and L. Maleki, "Chaotic dynamics of frequency combs generated with continuously pumped nonlinear microresonators," Opt. Lett. **38**, 525–527 (2013).
40. T. J. Kippenberg, S. M. Spillane, K. J. Vahala, "Kerr-nonlinearity optical parametric oscillation in ultrahigh-Q toroid microcavity," Phys. Rev. Lett. **93**, 083904 (2004).
41. L. A. Lugiato and R. Lefever, "Spatial dissipative structures in passive optical systems," Phys. Rev. Lett. **58**, 2209–2211 (1987).

#203476 - $15.00 USD Received 26 Dec 2013; revised 8 Feb 2014; accepted 13 Feb 2014; published 20 Feb 2014

42. T. Herr, V. Brasch, J. D. Jost, C. Y. Wang, N. M. Kondratiev, M. L. Gorodetsky, and T. J. Kippenberg, "Temporal solitons in optical microresonators," Nat. Photonics **8**, 145–152 (2014).
43. F. Leo, S. Coen, P. Kockaert, S. P. Goza, P. Emplit, and M. Haelterman, "Temporal cavity solitons in one-dimensional Kerr media as bits in an all-optical buffer," Nat. Photonics **4**, 471–476 (2010).
44. H. Lajunen, V. Torres-Company, J. Lancis, E. Silvestre, and P. Andres, "Pulse-by-pulse method to characterize partially coherent pulse propagation in instantaneous nonlinear media," Opt. Express **18**, 14979–14991 (2010).
45. M. Erkintalo and S. Coen, "Coherence properties of Kerr frequency combs," Opt. Lett. **39**, 283–286 (2014).
46. M. Haelterman, S. Trillo, and S. Wabnitz, "Additive-modulation-instability ring laser in the normal dispersion regime of a fiber," Opt. Lett. **17**, 745–747 (1992).
47. I. V. Barashenkov and Y. S. Smirnov, "Existence and stability chart for the ac-driven, damped nonlinear Schrodinger solitons," Phys. Rev. E **54**, 5707–5725 (1996).
48. F. Leo, L. Gelens, P. Emplit, M. Haelterman, and S. Coen, "Dynamics of one-dimensional Kerr cavity solitons," Opt. Express **21**, 9180–9191 (2013).
49. Y. K. Chembo, D. V. Strekalov, and N. Yu, "Spectrum and dynamics of optical frequency combs generated with monolithic whispering gallery mode resonators," Phys. Rev. Lett. **104**, 103902 (2010).
50. J. M. Dudley and S. Coen, "Coherence properties of supercontinuum spectra generated in photonic crystal and tapered fibers," Opt. Lett. **27**, 1180–1182 (2002).
51. J. M. Dudley, G. Genty, and S. Coen, "Supercontinuum generation in photonic crystal fibers," Rev. Mod. Phys. **78**, 1135–1184 (2006).
52. G. Genty, M Surakka, J. Turunen, and A. T. Friberg, "Second-order coherence of supercontinuum light," Opt. Lett. **35**, 3057–3059 (2010).
53. T. Godin, B. Wetzel, T. Sylvestre, L. Larger, A. Kudlinski, A. Mussot, A. Ben Salem, M. Zghal, G. Genty, F. Dias, and J. M. Dudley, "Real time noise and wavelength correlations in octave-spanning supercontinuum generation," Opt. Express **21**, 18452–18460 (2013).
54. G. P. Agrawal, *Nonlinear Fiber Optics*, 4th ed. (Academic, 2007).
55. M. R. E. Lamont, Y. Okawachi, and A. L. Gaeta, "Route to stabilized ultrabroadband microresonator-based frequency combs," Opt. Lett. **38**, 3478–3481 (2013).
56. K. Saha, Y. Okawachi, B. Shim, J. S. Levy, R. Salem, A. R. Johnson, M. A. Foster, M. R. E. Lamont, M. Lipson, and A. L. Gaeta, "Modelocking and femtosecond pulse generation in chip-based frequency combs," Opt. Express **21**, 1335–1343 (2013).
57. S. B. Papp, P. Del'Haye, and S. A. Diddams, "Parametric seeding of a microresonator optical frequency comb," Opt. Express **21**, 17615–17624 (2013).
58. M. Peccianti, A. Pasquazi, Y. Park, B. E. Little, S. T. Chu, D. J. Moss, and R. Morandotti, "Demonstration of a stable ultrafast laser based on a nonlinear microcavity," Nature Commun. **3**, 765 (2012).
59. P. Del'Haye, S. B. Papp, and S. A. Diddams, "Self-injection locking and phase-locked states in microresonator-based optical frequency combs," Phys. Rev. Lett. **112**, 043905 (2014).

1. Introduction

An optical frequency comb is a laser source with a spectrum composed by a set of evenly spaced components that maintain the phase coherence across the whole bandwidth. Thanks to the self-referencing technique for femtosecond mode-locked lasers [1, 2], it is now possible to synthesize/measure absolute optical frequencies with a performance level that before was only achievable by specialized laboratories [3]. This has led to a revolution in different fields, ranging from optical clocks to precision spectroscopy [4]. These applications mainly use mode-locked lasers, whose repetition rates are typically less than 10 GHz. There are other applications (such as optical arbitrary waveform generation, coherent optical communications or radio-frequency photonics) that do not require self-referencing but would benefit from higher repetition rates and smaller sized combs [5]. Recently, a novel platform has emerged with the prospect to achieve these two features simultaneously: the microresonator frequency comb [6].

In this new configuration, a continuous-wave (CW) laser pumps an ultrahigh-Q optical cavity. When the power builds up in the cavity, new frequency components are generated and interact by nonlinear mixing. The first demonstrations used whispering gallery mode resonators made of different materials including silica [7], CaF_2 [8], or MgF_2 [9]. More recently, microresonators were fabricated in planar geometries with high-index glass [10], silicon nitride [11] or AlN [12]. Here, the loaded Q factor of the cavities is lower ($\sim 10^5$–10^6 around 1.5 μm) but the nonlinear coefficients are sufficiently high to yield frequency combs, in some cases with thousands of

#203476 - $15.00 USD Received 26 Dec 2013; revised 8 Feb 2014; accepted 13 Feb 2014; published 20 Feb 2014

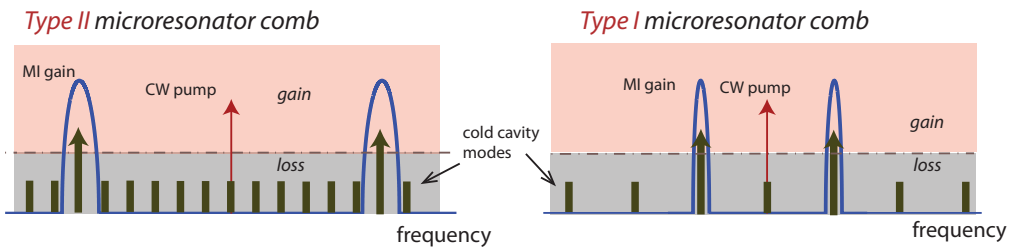

Fig. 1. Modulation instability (MI) is the underlying phenomenon that leads to parametric oscillation in microresonator frequency combs. In Type II combs, the MI sidebands generated by the CW pump lead to parametric growth of frequencies that are several FSRs away. These frequency components grow in power and nonlinear mix with the pump. This microresonator may lead to a spectrally partially coherent comb [29]. However, the comb dynamics can be altered by actively manipulating the CW pump settings in the course of comb formation. This may lead to the formation of stable combs [33, 39] and cavity solitons [42]. We show that these solutions are indeed stable and spectrally coherent, but they strongly depend on the particular initial conditions of the system. For Type I combs, the first oscillating modes are beside the pump and display a spectrally coherent behavior. These solutions are robust to the noise conditions.

modes and a bandwidth spanning tens of terahertz [13], similar to whispering-gallery-mode-based combs [14]. The appeal of microresonator frequency combs is that the repetition rate is governed by the free spectral range (FSR) of the cavity (and can thus be significantly higher than femtosecond mode-locked lasers) and the gain bandwidth is "man-made", in the sense that it can be controlled via dispersion engineering [15–19] within the transparency window of the cavity material [20–22]. In addition, the manufacturing process of microresonators with silicon nitride and high-index material is compatible with CMOS fabrication standards [23] and thus it is not difficult to envision embedding more subsystems onto the same chip with additional engineering effort.

However, before realizing the full potential of this novel platform one must ensure that the requirement of full coherence across the bandwidth is indeed satisfied. Strikingly, recent experiments by Weiner and colleagues [24] and Papp and Diddams [25] revealed that this is not always the case. They focused on getting transform-limited pulses from microresonator combs by line-by-line pulse shaping [26]. Following the nomenclature of [24], there was a clear distinction between the noise performance exhibited by combs where the spectral distance between the CW pump laser and the first oscillating frequencies in the comb corresponded to one (Type I) or more (Type II) cavity's FSRs (see Fig. 1) [24, 27–29]. The former class allows for getting transform-limited pulses after phase compensation: an indirect indication of spectrally coherent behavior. For Type II combs and for certain pump setting conditions, it was not possible to achieve transform-limited pulses. This led to a degradation in the peak to background ratio in the measured autocorrelation trace when compared to the corresponding digitally compressed one [24, 25]. The explanation for this phenomenon was that the spectral phases of the microresonator comb were fluctuating randomly over a certain range (see supplementary information from [24]). Different groups have reported similar observations. Recent multi-heterodyne experiments showed that Type II combs operating in the partially coherent regime do not have a spectrum formed by evenly spaced frequency components, leading to decreased noise performance as inferred by the broadening of the RF beat note of the microresonator comb [29]. An important conclusion is that neither the formation dynamics nor the noise behavior is exclusive of a particular material or geometry [29]. In [25, 28], it was observed that when the RF beat

#203476 - $15.00 USD Received 26 Dec 2013; revised 8 Feb 2014; accepted 13 Feb 2014; published 20 Feb 2014

note appears broadened, the comb light couldn't be temporally compressed. This has a strong implication in optical communications because this apparent lack of spectral coherence leads to degradation in the bit error rate performance when the comb is used as a multiwavelength transmitter [28].

One can find in the literature physical analyses that provide quantitative insight into the formation of microresonator combs [30–39], including approximate analytical [30, 32, 36, 40] and numerical solutions [31], as well as stability studies [33, 37–39]. It has been recognized that the essential physics of the microresonator combs (excluding modal crossing and mechanical and thermal effects) can be described by a master equation [32, 34, 35], mathematically isomorphic to the one derived by Lugiato and Lefever in the framework of spatial solitons and pattern formation in cavities [41]. Likewise, temporal cavity solitons have been observed and analyzed in microresonator frequency combs [42] and fiber-based cavities (see e.g. [43]). Notwithstanding, comparatively few efforts have been devoted towards a better theoretical understanding of the noise formation in general (and the coherence properties in particular) in microresonator frequency combs. This is a challenging task, since a thorough stochastic analysis requires computing thousands of ensemble realizations upon propagation in an instantaneous nonlinear system [44]. However, the random nature of light cannot be ignored since it is at the core of the formation of the microresonator comb. The spontaneous generation of frequency components in the cavity primarily arises by parametric amplification of vacuum fluctuations [30, 40], i.e. modulation instability (MI).

Regarding coherence studies in microresonator combs, Erkintalo and Coen [45] have analyzed numerically the first-order-degree of spectral coherence when the comb is operating under different regimes, which are linked to the solutions of the Lugiato-Lefever equation [38]. They find that stable and coherent spectra can be obtained in Type II combs at either the onset of modulation instability or when cavity solitons are formed [45]. Here, we complement this study by analyzing the connection between spectral coherence and the dynamics of Type I versus Type II microresonator combs. In line with recent observations [24, 25, 27, 28], we also find that Type II combs are coherent as long as the oscillating modes remain incapable to provide net MI gain by themselves. Otherwise, we observe a degradation of the coherence, but only in particular regions of the spectrum. We also find that cavity solitons are stable and spectrally coherent but these solutions are susceptible to the vacuum fluctuations that drive the dynamics of the comb. The most important observation of our work is that Type I combs emerge in a natural manner and are indeed spectrally coherent, regardless of the initial seed conditions. This work highlights the relevance of reporting stability, shot-to-shot fluctuations, spectral coherence and repeatability in microresonator comb experiments.

2. Parametric oscillation revisited in the framework of the Lugiato-Lefever equation

The starting point of the next analysis is the Lugiato-Lefever equation (LLE) [41]. As mentioned in the introduction, this equation has been used previously to describe modulation instability and soliton dynamics in CW-pumped fiber cavities [46–48] and microresonator combs [32, 34, 35]. For the sake of completeness, we summarize here the physics of parametric oscillation that we find more relevant in determining the coherence properties of microresonator combs. More extensive analyses can be found in [32, 36–38, 46].

The LLE reads as

$$t_R \frac{\partial E(t,\tau)}{\partial t} = \left[-\alpha - i\delta_0 + iL \sum_{k\geq 2} \frac{\beta_k}{k!} \left(i\frac{\partial}{\partial \tau} \right)^k + i\gamma L |E(t,\tau)|^2 \right] E(t,\tau) + \sqrt{\theta} E_{\text{in}} . \qquad (1)$$

Here, $E(t,\tau)$ describes the complex field envelope inside the ring cavity, with the time τ accounting for waveform variations within the roundtrip time t_R, whereas t is a *slow* time vari-

#203476 - $15.00 USD Received 26 Dec 2013; revised 8 Feb 2014; accepted 13 Feb 2014; published 20 Feb 2014

able related to the field evolution in succesive roundtrips. L is the cavity length; α the loss per roundtrip, i.e. $\alpha = (\alpha_i L + \theta)/2$, with α_i being the propagation loss per unit length, and θ the transmission power coefficient in the cavity coupler; δ_0 is the phase detuning of the CW pump frequency, ω_p, with respect to the closest cavity resonance, ω_0, i.e. $\delta_0 = t_R(\omega_0 - \omega_p)$. The dispersion coefficients are given by β_k, where β_2 is the lowest-order one, describing the group velocity dispersion, and the nonlinear coefficient is γ. Finally, E_{in} accounts for the complex field of the CW pump. The cavity's mean free spectral range is $\text{FSR} = 1/t_R$. It is worth reminding that for low propagation loss and under critical coupling condition, $\alpha = \theta$, the loaded quality factor is related to the roundtrip loss by $Q = \omega_0/(2\alpha\text{FSR})$.

Parametric oscillation in microresonators is analyzed by probing the LLE with the ansatz $E(t,\tau) = a_{(-)}\exp(-i\Omega\tau) + a_0 + a_{(+)}\exp(i\Omega\tau)$ [36, 46], where $a_{(-)}$ and $a_{(+)}$ are much smaller than a_0, and this last term satisfies the optical bistability equation $a_0\left[\alpha + i\left(\delta_0 - \gamma L P_0\right)\right] = \sqrt{\theta}E_{\text{in}}$, where $P_0 = |a_0|^2$. It is easy to show that in a first-order-dispersion approximation the LLE presents exponentially growing solutions for $a_{(-)}$ and $a_{(+)}$, proportional to $\exp\left[\Lambda(\Omega)t\right]$ [46]. The gain coefficient is $\Lambda(\Omega) = -\alpha + \sqrt{(\gamma L P_0)^2 - (\Delta\kappa(\Omega))^2}$ and is maximum when the phase-mismatch $\Delta\kappa(\Omega) = \delta_0 - L\beta_2\Omega^2/2 - 2\gamma L P_0$ equals zero. This occurs at the angular frequency [46]

$$\Omega_{\text{m}}^2 = \frac{2}{L\beta_2}\left(\delta_0 - 2\gamma L P_0\right). \tag{2}$$

At this frequency, the modes $a_{(-)}$ and $a_{(+)}$ will experience net gain as long as $P_0 > P_{0,\text{th}} = \alpha/(\gamma L)$, which defines the required power threshold for parametric oscillation. Considering the optical bistability condition, the above threshold for the intracavity power provides the CW pump power needed to achieve parametric oscillation,

$$P_{\text{in,th}} = \frac{1}{\gamma L}\left[\alpha^2 + (\delta_0 - \alpha)^2\right], \tag{3}$$

where critical coupling is assumed. Parametric oscillation in microresonator combs has been previously studied [30, 40]. It is interesting to note that the $1/Q^2$ dependence in the required threshold pump power (see e.g. Eq. (10) in [30]) can alternatively be obtained in the framework of the LLE. In particular, if we take Eq. (3) and consider $\delta_0 = 0$, the pump power threshold becomes $P_{\text{in,th}} = 2\alpha^2/(\gamma L)$, in agreement with [49]. Note that this threshold is different from the absolute parametric threshold, which is given for a fixed pump power when the detuning satisfies [38]

$$\delta_0 \geq \alpha - \sqrt{P_{\text{in}}\gamma L - \alpha^2}. \tag{4}$$

As firstly observed in [24, 27–29], microresonator combs whose first oscillating frequencies appear one FSR away from the pump appear to be stable and admit compressibility to the transform-limited duration [24]. Thus, it is important to assess the design rules that lead to this type of microresonator comb (so-called Type I [24, 27, 28]). From Eq. (2), the Type I condition, i.e. $\Omega_{\text{m}} = 2\pi\text{FSR}$, imposes the dispersion of the cavity to satisfy

$$\beta_2 = \frac{\left(\delta_0 - 2\gamma L P_0\right)}{2L\pi^2\text{FSR}^2}. \tag{5}$$

This indicates that, depending on the cavity detuning, either normal or anomalous dispersion may lead to Type I combs. For zero detuning and considering the intracavity power at threshold, $P_{0,\text{th}}$, we get $\beta_2 = -\alpha/(L\pi^2\text{FSR}^2)$ (in close agreement to what is found in [29]), which means that anomalous dispersion is required. Equation (5) can be considered as a generalization for the Type I design rule, where P_0 is not necessarily the intracavity power at threshold.

In the following sections, we shall verify that spectrally coherent combs are achievable for Type I combs. For completeness, these results are benchmarked to the coherence properties of

#203476 - $15.00 USD Received 26 Dec 2013; revised 8 Feb 2014; accepted 13 Feb 2014; published 20 Feb 2014

Type II combs whose detuning is just above the minimum defined by Eq. (4) [45], or temporal cavity solitons.

3. Numerical results

The spectral coherence of microresonator combs is evaluated by means of the following figure of merit [45]

$$|g(\omega;t_1,t_2)| = \frac{\left|\langle \tilde{E}^*(t_1,\omega)\tilde{E}(t_2,\omega)\rangle\right|}{\langle\left|\tilde{E}(\omega)\right|^2\rangle}. \tag{6}$$

Here, the complex field $\tilde{E}(t,\omega)$ is the Fourier transform of $E(t,\tau)$ with respect to τ. The frequency dependence of the two-time correlation function has been widely used to assess the noise performance of different supercontinuum sources [50,51]. Different figures of merit, e.g. the two-frequency correlation function [52] or higher-order correlations [53] can be studied too, but this is a topic beyond the scope of this work.

The brackets above denote ensemble averaging. In practice, we solve Eq. (1) starting from an empty ring. The waveform $E(t,\tau)$ is calculated within the temporal window $-t_R/2 \leq \tau \leq t_R/2$, and the steps taken in the variable t correspond to a single cavity roundtrip time. Before every step, we load the CW pump with statistically independent noise consisting of one photon per spectral bin with random phase [50, 51]. We calculate the complex degree of coherence at a fixed time difference $t_2 - t_1$ and 1000 different instants t_1 of the evolution time. As demonstrated in [45], for time differences shorter or in the order of the photon lifetime in the cavity, $t_{\rm ph} = t_R/(2\alpha)$, the light source may display coherent behavior even in a regime where the comb is inherently unstable. In order to avoid these artifacts, we choose $t_2 - t_1$ to be more than one order of magnitude longer than $t_{\rm ph}$.

3.1. Example A: Type II microresonator comb

In our first example, the microresonator is designed with FSR = 226 GHz, $L = 2\pi r$ with $r = 100\,\mu$m, $\alpha = \theta = 0.003$, $\gamma = 1000\,(\text{W}\cdot\text{km})^{-1}$, $\beta_2 = -48.5\,\text{ps}^2/\text{km}$, $\beta_3 = 0.131\,\text{ps}^3/\text{km}$ and $\beta_4 = 0.0025\,\text{ps}^4/\text{km}$. These parameters could be realistically obtained with a silicon nitride microresonator and are similar to the ones reported in [13,35]. We consider a CW pump power of 1.5 W. From Eq. (4), the required detuning for parametric oscillation is $\delta_0 \geq -0.028$. In Fig. 2 we plot the dynamics of the microresonator comb at different detuning values satisfying the above inequality. For values close to the threshold [see Fig. 2(a)], only a few discrete frequency components are generated. In a first step, the pump generates two new frequencies through degenerate four-wave mixing [6, 29], that is the fundamental interaction behind the modulation instability process [54]. The position of these lines corresponds to the frequencies $\pm\Omega_{\rm m}$ given by Eq. (2) and are $\pm 2\pi \times 6.7$ THz in this case, much higher than the cavity's FSR. In a second step, these three frequencies interact through a nondenegerate and stimulated four-wave mixing process. Consequently, new frequencies appear at $\pm 2\Omega_{\rm m}$ and $\pm 3\Omega_{\rm m}$, keeping in this way the equidistance between lines [6, 29]. We observe that the comb evolves towards a stable steady state after several roundtrips. Pulses are formed as soon as the new frequencies emerge. Figure 2(b) displays the comb dynamics for the case in which the CW pump is closer to resonance. Here there is an initial state similar to the case in Fig. 2(a), but the first oscillating modes acquire sufficient power to stimulate the growth of frequency components located between them and the pump through a degenerate four-wave-mixing process [27,29,55]. These new lines generate more frequency components by non-degenerate and stimulated four-wave-mixing processes. In the time domain, the mixing leads to strong intensity variations. Finally, in the case in which the comb is initiated by pumping on resonance, Fig. 2(c), a broader microresonator comb is rapidly obtained, and the spectrum fills quickly all the FSRs between the pump and the first oscillating

#203476 - $15.00 USD Received 26 Dec 2013; revised 8 Feb 2014; accepted 13 Feb 2014; published 20 Feb 2014

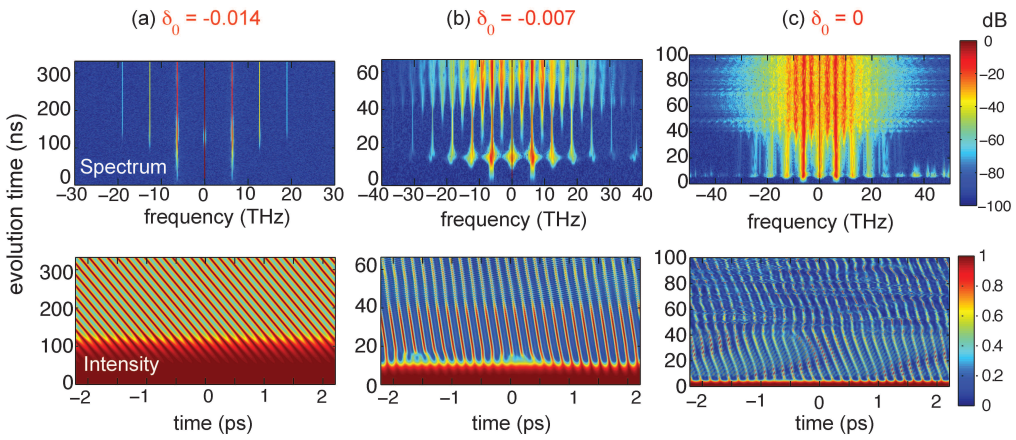

Fig. 2. Dynamics of a Type II microresonator comb in spectral domain (top row) and time domain (bottom row) for different detuning conditions. Corresponding average spectra, shot-to-shot fluctuations and spectral coherence are displayed in Fig. 3.

modes. However, the waveform does not approach a steady state and there are strong spectral and intensity variations from one roundtrip to the next.

We have calculated the spectral coherence for each example above as per Eq. (6) and the results are presented in Fig. 3. For each detuning, the evolution of the waveform over the variable t is calculated over long time distances. As explained before, the coherence is calculated for pairs of spectral waveforms separated $t_2 - t_1 > 10t_{\mathrm{ph}}$. In order to get conclusive statistics, we compute 1000 consecutive pairs. The evolution of the field over time is shown on the left column in Fig. 3. On the right column, the field realizations are superimposed and the average spectrum corresponding to the comb envelope is calculated and shown in pink. For $\delta_0 = -0.014$ in Fig. 3(a), the fluctuations appear only at the background level and the comb displays a spectrally coherent behavior. The MI lines remain highly coherent and stable upon evolution. For detuning values closer to resonance, $\delta_0 = -0.007$ in Fig. 3(b), the spectral regions around the first oscillating modes remain coherent, however the new comb lines that arise in between are partially coherent. One can indeed observe stronger amplitude fluctuations in these spectral regions and conclude that the comb is spectrally partially coherent. Finally, right on resonance, $\delta_0 = 0$ in Fig. 3(c), the spectral envelope of the combs is much smoother but there appear large spectral fluctuations from shot to shot that lead to a degradation of the spectral coherence across the whole bandwidth. These findings are in agreement with the analysis carried out in [45] based on the stability of the LLE solutions.

3.2. *Example B: Type I microresonator comb*

We now consider a slightly different microresonator, with design parameters FSR $= 2.41$ THz, $r = 10\,\mu$m, $\alpha = \theta = 0.001$, $\gamma = 1100\,(\mathrm{W{\cdot}km})^{-1}$ and $\beta_2 = -623.4\,\mathrm{ps}^2/\mathrm{km}$. These parameters are chosen so that Eq. (5) is satisfied at resonance for a CW pump power of 0.2 W. The field evolution is calculated in the same manner as before. Likewise, the complex degree of coherence is computed for a fixed time difference greater than $10t_{\mathrm{ph}}$. The average spectral envelopes and degrees of coherence are displayed in Figs. 4(a)–4(d) for different pump powers but keeping $\delta_0 = 0$.

The comb is always highly coherent in this case. The broadest comb envelope corresponds to the case in which the MI gain peak matches the FSR of the cold cavity, as Fig. 4(e) indicates. Under the spectral envelope figures, we plot the corresponding intensity profile (temporally

#203476 - $15.00 USD Received 26 Dec 2013; revised 8 Feb 2014; accepted 13 Feb 2014; published 20 Feb 2014

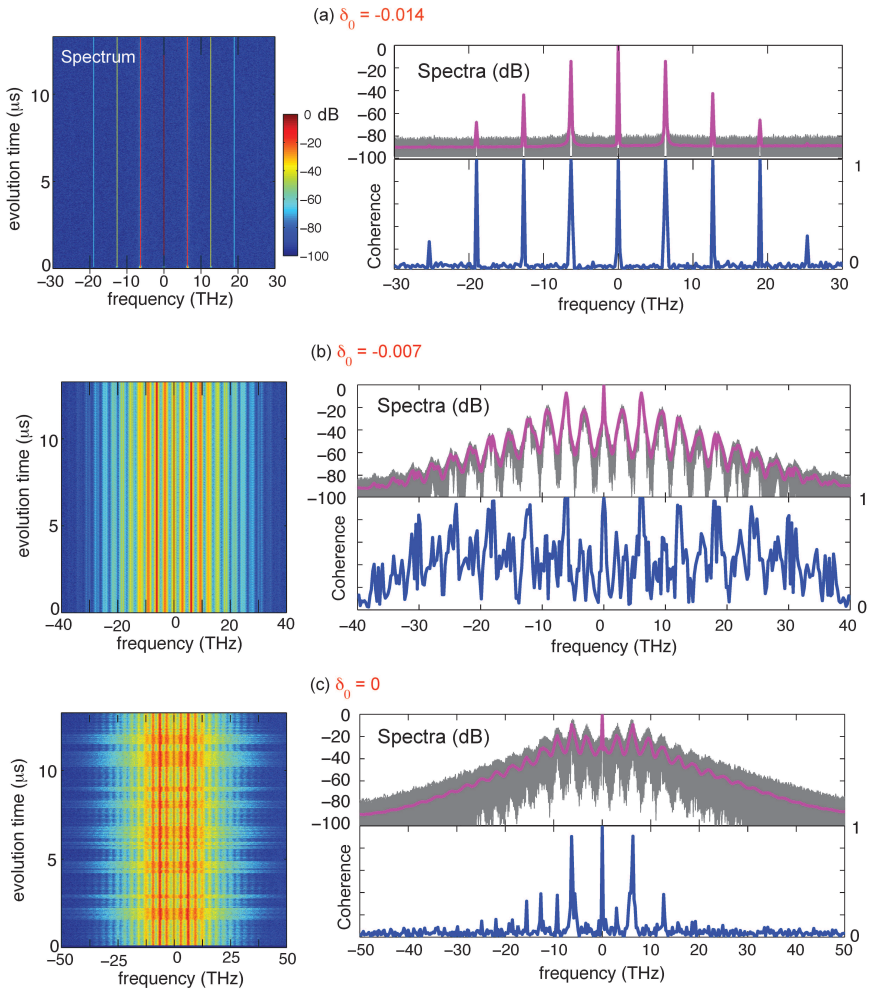

Fig. 3. Spectral coherence and shot-to-shot fluctuations for the microresonator combs in Fig. 2.

shifted for clarity) and compare it to the transform-limited case. For the optimum case in which $P_{\text{in}} = 0.2\,\text{W}$, the pulse is very close to the transform limit. For higher powers [Figs. 4(c) and 4(d)], the pulse deviates from the optimally compressed case, yet the degree of coherence is 1. This means that the spectral phase is not uniform but high-quality ultrashort pulses can be achieved with the aid of a line-by-line pulse-shaping device [24].

It is interesting to investigate whether the system approaches the above steady state regardless of the input noise conditions. To answer this, we compute a slightly different degree of coherence

$$|g_s(\omega;t)| = \frac{\left|\langle \tilde{E}_1^*(t,\omega)\tilde{E}_2(t,\omega)\rangle\right|}{\sqrt{\langle\left|\tilde{E}_1(\omega)\right|^2\rangle\langle\left|\tilde{E}_2(\omega)\right|^2\rangle}}. \tag{7}$$

Here, the pair of waveforms $\tilde{E}_1(t,\omega)$ and $\tilde{E}_2(t,\omega)$ are calculated at a fixed instant time t for different random seeds. We note that this magnitude is conceptually closer to the one considered when evaluating the coherence properties in supercontinuum fiber sources [50, 51], where the

#203476 - $15.00 USD Received 26 Dec 2013; revised 8 Feb 2014; accepted 13 Feb 2014; published 20 Feb 2014

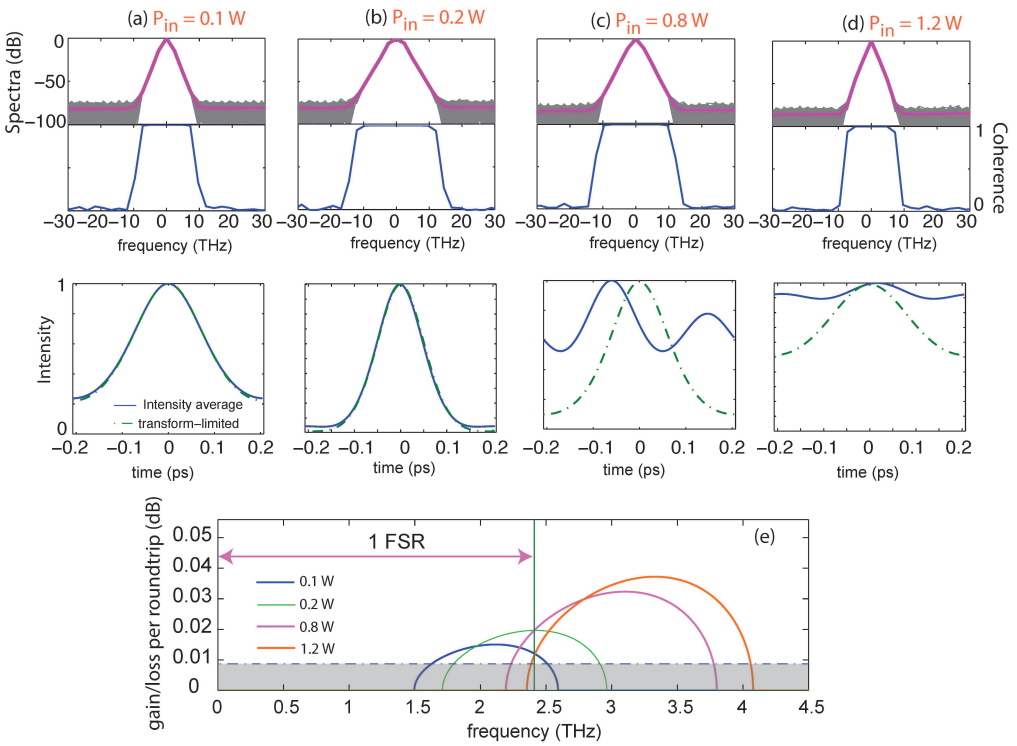

Fig. 4. (a)-(d) Average envelope spectra, degree of coherence and intensity profile for a Type I microresonator comb at different pump power leves. (e) MI gain bandwith shift for different power levels. At 0.2 W the maximum gain coincides with the FSR of the microresonator cavity.

different realizations calculated for the ensemble average are evaluated for a fixed fiber length and considering different random seeds. Our findings are summarized in Fig. 5 for the case of Fig. 4(b). In order to make sure that the system has approached the steady state we are considering $t = 10000\,t_{\mathrm{ph}}$. As in the previous case, we compute 1000 random seeds to calculate the average in Eq. (7). All the spectra are superposed (gray curves) and the average spectrum is shown in pink solid line. We observe that the spectral envelope of the comb remains constant in amplitude and is almost identical to the one calculated by averaging, for a single random seed, over multiple roundtrip times [pink solid line in Fig. 4(b) here displayed as dashed yellow]. However the degree of coherence as defined by Eq. (7), shown in dashed blue curve under the spectrum, indicates a highly incoherent behavior for all the frequency components except for the pump. What occurs is that the pulses achieve the same temporal profile as in Fig. 4(b) but appear randomly delayed within the cavity period for different random seeds. This leads to identical spectra with a linear spectral phase ramp with random slope. When the delay is compensated *offline*, we observe a substantial increase in the spectral coherence as defined by Eq. (7) (blue solid line). This curve indeed matches the degree of coherence as calculated by Eq. (6), which is displayed for completeness in red dashed line in Fig. 5.

The conclusion from the above findings is that, apart from an irrelevant arbitrary delay, Type I combs approach a steady state coherent solution regardless of the input noise seed. As shall be seen in the next section, this conclusion needs to be refined in the context of temporal cavity solitons.

#203476 - $15.00 USD Received 26 Dec 2013; revised 8 Feb 2014; accepted 13 Feb 2014; published 20 Feb 2014

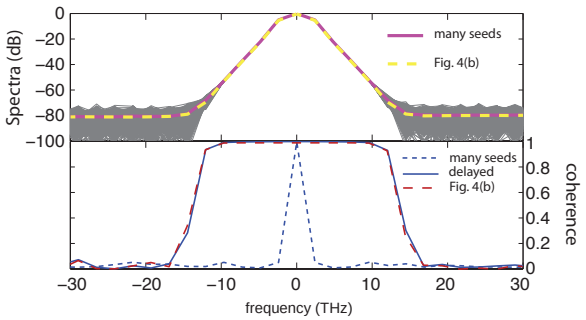

Fig. 5. Analysis of the universality of the stable solutions for Type I coherent combs. (Top) The different realizations calculated at a fixed instant time for different random seeds. (Bottom) the degree of coherence calculated at fixed time t over multiple noise seeds (blue dash curve) is however substantially different when compared to the one calculated at multiple instant times for a fixed seed (red dash curve). After compensating for a linear spectral phase ad hoc, the degree of coherence calculated at a fixed time for various noise seeds (blue solid line) is identical to the degree of coherence calculated for a fixed seed and various instant times.

4. Stability and coherence of temporal cavity solitons

In the examples in the previous section, we have considered the evolution of the system for a fixed pump power and detuning. This is what in the literature is known as the soft excitation regime [33,36]. Notwithstanding, Eq. (1) admits different mathematical solutions that are physically stable too. However, in order to gain access to these states, one must vary dynamically either the pump power or the detuning in the course of comb formation. This is what is called the hard excitation regime [33, 36, 39]. Several groups have reported stable combs achieved in this manner (see, e.g. [13, 29, 56]). One of the more impressive results of stable microresonator combs in this regime corresponds to the case of temporal cavity solitons [42]. The transition towards temporal cavity solitons (CSs) has been also studied numerically [38, 42, 55]. In [38], it was evidenced that the comb evolves from an initial MI stage through a chaotic regime to finally provide temporal CSs. This has been proved numerically by studying the evolution of the comb by inducing abrupt detuning transitions [55]. By analyzing the LLE solutions in the above-mentioned stages, it appears clear that the comb losses spectral coherence in the transition from MI to the chaotic regime, but it recovers the stability after entering the regime where cavity solitons are formed [45].

In this section we study the formation of CSs by solving the LLE. The microresonator parameters are the same as described in Sect. 3.1. For simplicity we keep only the first-order-dispersion. Instead of forcing abrupt changes in detuning parameter, we ramp it in a continuous manner. As in the previous sections, the CW pump and noise are added every roundtrip. This procedure is closer to the experimental implementations, where the laser frequency is swept continuously around the cavity resonance [42]. The programmed dynamic detuning is depicted in Fig. 6(a). We first set $\delta_0 = -0.025$ for a time duration corresponding to $120 t_{\mathrm{ph}}$. The comb remains here in the stable MI stage [as indicated by Eq. (4)]. We then sweep linearly in time the detuning for $120 t_{\mathrm{ph}}$ more until it reaches $\delta_0 = 0.070$. We note that this value lies within the range $3(P_{\mathrm{in}}\gamma L\alpha/4)^{1/3} \leq \delta_0 \leq \pi^2 P_{\mathrm{in}}\gamma L/(8\alpha)$, where CSs are expected to form [38]. This continuous ramping is different to the one evaluated in [55], but as Figs. 6(b) and 6(c) illustrate, we reach the same conclusions: upon the initial MI stage, the comb enters into a chaotic regime, with large spectral broadening but loss of temporal structure. Then, the comb moves towards

#203476 - $15.00 USD Received 26 Dec 2013; revised 8 Feb 2014; accepted 13 Feb 2014; published 20 Feb 2014

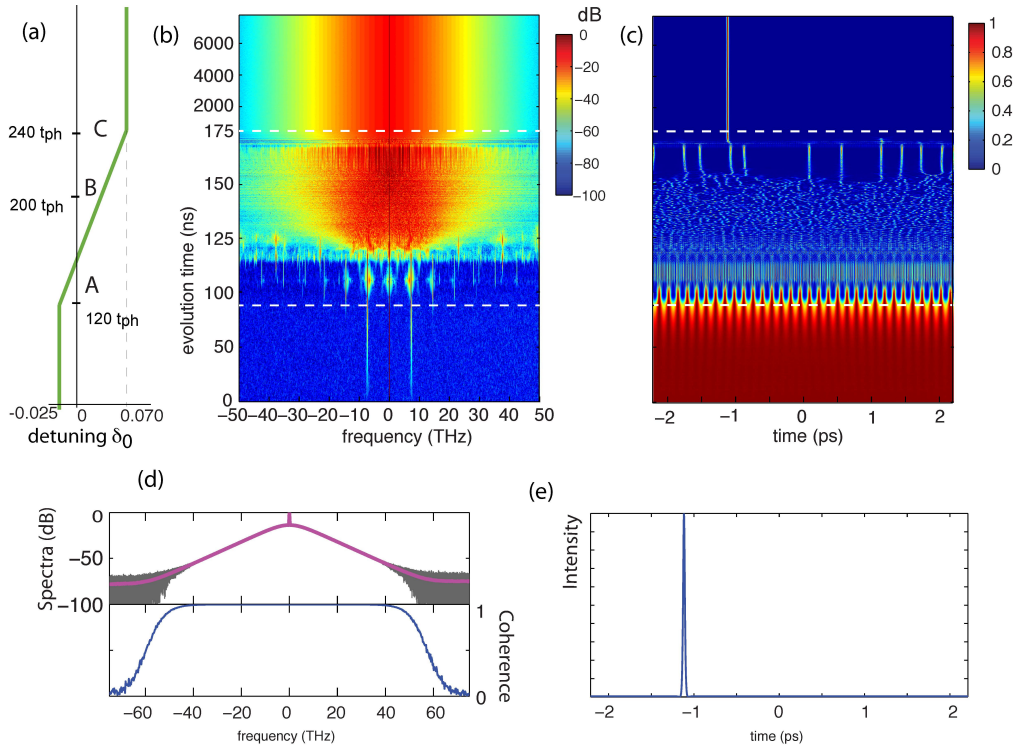

Fig. 6. Temporal cavity soliton formation in microresonators. (a) Dynamic evolution of detuning. Corresponding (b) spectral and (c) time domain evolutions. Note the difference in time scales at different stages. The detuning is changed dynamically in the course of the CS formation. In the first stage, it is kept constant. The points marked as A and C are indicated by the dashed white lines in (b) and (c). Once the cavity soliton is formed, the waveform appears stable and coherent (d). The average intensity indicates a pulse with 25 fs duration (e).

a stage where only a few pulses oscillate per period. After continuous detuning, these waveforms collapse into a stable pulse. In order to get sufficient statistics to calculate the spectral coherence, once this pulse is formed, we let the waveform evolve further in time while keeping the detuning constant. In order to compute Eq. (6), we store 1000 waveforms separated by $10t_{\mathrm{ph}}$ from each other. Snapshots in time and frequency at the relevant regimes are shown in Fig. 7. Our analysis of the spectral coherence reveals that the cavity pulse is highly coherent [Fig. 6(d)], confirming what has been recently found by analyzing the LLE solutions [45].

Next, we are interested in the robustness of this solution for different noise seeds, for which we repeat the above simulation considering the same microresonator parameters, including the sweep and pump power. The only difference now is the set of independent random noise seeds accompanying the CW pump every roundtrip, which is otherwise inaccessible by any experimental means. Interestingly, the system achieves a different steady state consisting of two temporal cavity solitons. This waveform also has a high degree of spectral coherence. Figure 7 compares the relevant waveforms in time and frequency domains obtained at particular instant times for the two sets of noise considered. In the initial MI stage, the waveforms are almost identical, simply shifted in time. However, the waveform achieved in the chaotic stage [indicated as time B in Fig. 7] is different. When the system achieves the steady state, the exact

#203476 - $15.00 USD Received 26 Dec 2013; revised 8 Feb 2014; accepted 13 Feb 2014; published 20 Feb 2014

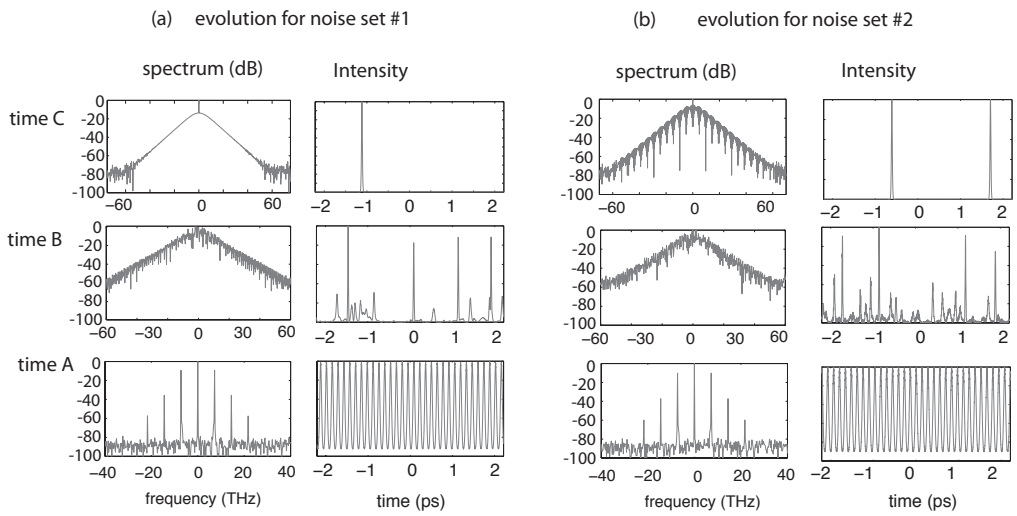

Fig. 7. Analysis of cavity soliton formation under different noise conditions. The sweep and other parameters are identical to those in Fig. 6. The points A-C are indicated in Fig. 6(a).

waveform depends on the set of noise seeds accompanying the pump every roundtrip. In the case presented in Fig. 7(b) it shows two solitons but in other runs the system evolves towards 1, 2, 3, 4, 5 solitons or simply collapses into a continuous wave. We know that the conclusion depends on the particular ramp programmed. Whether the system evolves to a single soliton regardless the noise conditions for an optimal ramp choise is an open question.

Such a fine sensitivity of CSs to the particular noise conditions has been observed experimentally [42] and discussed in [42, 45]. An expression for the maximum number of stationary (non interacting) CSs is provided in [42]. It is important to note [42] that the condition to get a maximum number of solitons equal to 1 coincides with the design rule for Type I microresonators [29].

5. Conclusions and discussion

We have analyzed the spectral coherence of microring resonator combs. There is a strikingly different behavior between Type I and Type II combs. In the soft excitation regime, Type II combs are spectrally coherent just at the onset of parametric oscillation, where only the primary lines oscillate and mix with the CW pump. The spectral coherence is severely degraded when the spectral gap between these lines and the CW pump fills in.

This type of combs may however admit the formation of temporal cavity solitons. This requires operating the microresonator in the hard excitation regime by, e.g., realizing a proper detuning of the CW pump in the course of comb formation. We showed that CSs are spectrally coherent and stable, but their formation is very sensitive to vacuum fluctuations. On the contrary, when the microresonator is designed to provide Type I combs, the system always approaches a steady state, stable, spectrally coherent solution regardless of the noise conditions.

We wish to emphasize that the above are not the only possibilities to achieve microresonator combs operating in a high-coherence state. As recent experiments indicate, stable microresonator combs can be obtained by pumping with a waveform composed of multiple CW waves (parametric seeding) [57], or by placing the microring in a fiber cavity [58]. Other observations leading to low-noise states show features akin to injection locking between ensembles of comb modes [59]. Further numerical and experimental work is needed to understand the spectral co-

#203476 - $15.00 USD Received 26 Dec 2013; revised 8 Feb 2014; accepted 13 Feb 2014; published 20 Feb 2014

herence for these new mechanisms and provide general design rules for self-starting spectrally coherent microresonator combs.

Acknowledgments

Victor Torres acknowledges stimulating discussions with Prof. A. M. Weiner. This work has been partly funded by the Swedish Research Council (VR), by the Plan Nacional I+D+I under the research project TEC2008-05490, Ministerio de Ciencia e Innovación (Spain), and by the Generalitat Valenciana under the grant PROMETEO 2009-077. David Castelló-Lurbe gratefully acknowledges funding from the Generalitat Valenciana (VALi+d predoctoral contract).

#203476 - $15.00 USD Received 26 Dec 2013; revised 8 Feb 2014; accepted 13 Feb 2014; published 20 Feb 2014